

# Anisotropic Exchange Interactions of Spin-Orbit-Integrated States in $\text{Sr}_2\text{IrO}_4$

Hosub Jin,<sup>1</sup> Hokyun Jeong,<sup>2</sup> Taisuke Ozaki,<sup>3</sup> and Jaejun Yu<sup>1,4,\*</sup>

<sup>1</sup>*Department of Physics and Astronomy and Center for Strongly Correlated Materials Research, Seoul National University, Seoul 151-747, Korea*

<sup>2</sup>*Computational Science and Technology Interdisciplinary Program, Seoul National University, Seoul 151-747, Korea*

<sup>3</sup>*Research Center for Integrated Science, Japan Advanced Institute of Science and Technology, Nomi, Ishikawa 923-1292, Japan*

<sup>4</sup>*Center for Theoretical Physics, Seoul National University, Seoul 151-747, Korea*

(Dated: February 20, 2024)

We present a microscopic model for the anisotropic exchange interactions in  $\text{Sr}_2\text{IrO}_4$ . A direct construction of Wannier functions from first-principles calculations proves the  $j_{\text{eff}}=1/2$  character of the spin-orbit integrated states at the Fermi level. An effective  $j_{\text{eff}}$ -spin Hamiltonian explains the observed weak ferromagnetism and anisotropy of antiferromagnetically ordered magnetic state, which arise naturally from the  $j_{\text{eff}}=1/2$  state with a rotation of  $\text{IrO}_6$  octahedra. It is suggested that  $\text{Sr}_2\text{IrO}_4$  is a unique class of materials with effective exchange interactions in the spin-orbital Hilbert space.

## I. INTRODUCTION

Many of transition metal oxides (TMOs) are antiferromagnetic insulators. The simplest model for such Mott insulators is the Hubbard model Hamiltonian,<sup>1</sup> which gives rise to an effective exchange term called superexchange interaction at half-filling. When orbital degrees of freedom are involved, a variety of exchange interactions can occur for a given ionic configuration with different crystal structures. In the case of colossal magneto-resistance manganese oxides, for instance, the superexchange interaction with orbital degeneracy determines complex spin and orbital orderings and, when doped, degenerate  $e_g$  orbitals coupled to the lattice via Jahn-Teller interactions become an essential part of the double exchange physics<sup>2</sup>. Sometimes the orbital degrees of freedom via spin-orbit (SO) coupling are responsible for the magnetic anisotropy bound to the crystal environment. When there exists an orbital degeneracy, SO coupling may become a dominant term so that the effective Hamiltonian should involve the full spin-orbital Hilbert space where the ground state must comply with the intersite spin and orbital correlations<sup>3</sup>. A possible dynamic interference between the spin and orbital space was suggested in vanadates<sup>4</sup>. There was a report of a large spin-orbital fluctuations in Mott insulators with  $t_{2g}$  orbital degeneracy as a manifestation of quantum entanglement of spin and orbital variables<sup>5</sup>.

Recently we have shown that the electron correlation effect combined with strong spin-orbit (SO) interactions is responsible for the observed insulating behavior of 5d TMO  $\text{Sr}_2\text{IrO}_4$ <sup>8</sup>. While SO coupling has been considered as a minor perturbation in the description of magnetism<sup>6</sup>, the amount of SO interactions in 5d elements including Ir, for example, is an order of magnitude larger than in the 3d TMO system<sup>7</sup>. Thus the SO coupling is expected to play a significant role in the electronic and magnetic properties of 5d TMO systems. Indeed the manifestation of a novel  $j_{\text{eff}}=1/2$  Mott ground state in  $\text{Sr}_2\text{IrO}_4$  was revealed by angle resolved photoemission spectroscopy, optical conductivity, x-ray absorption spectroscopy measurements, and first-principles electronic structure calculations<sup>8</sup>. Further investigations of the electronic structures of the  $\text{Sr}_{n+1}\text{Ir}_n\text{O}_{3n+1}$  ( $n = 1, 2$ , and  $\infty$ ) series

demonstrated a Mott insulator-metal transition with a change of bandwidth as  $n$  increases<sup>9</sup>. The ground state of 5d TMO  $\text{Sr}_2\text{IrO}_4$  is a Mott insulator in the strong spin-orbit coupling limit. In addition,  $\text{Sr}_2\text{IrO}_4$  exhibits unusual weak ferromagnetism with reduced Ir magnetic moments<sup>10,11,12,13,14</sup>. To understand such unusual magnetic properties of  $\text{Sr}_2\text{IrO}_4$ , it is necessary to take account of the spin-orbit integrated  $j_{\text{eff}}=1/2$  state.

In this paper, we introduce a prototype model of spin-orbit-integrated magnetism realized in  $\text{Sr}_2\text{IrO}_4$ . From a tight-binding analysis based on first-principles calculations, we show that the  $j_{\text{eff}}=1/2$  character of the spin-orbit-integrated state remains robust even in the presence of on-site Coulomb interactions. A direct construction of Wannier functions from first-principles calculations proves the  $j_{\text{eff}}=1/2$  character at the Fermi level. An effective exchange Hamiltonian with not  $S=1/2$  but  $j_{\text{eff}}=1/2$  is obtained starting from a  $j_{\text{eff}}=1/2$  Hubbard model. The origin of anisotropic magnetic exchange interactions are discussed in connection with an extraordinary character of the ground state. The presence of spin-orbit-integrated state with strong SO interactions in  $\text{Sr}_2\text{IrO}_4$  can make 5d Ir-oxides a unique class of materials for the study of effective exchange interactions in the full spin-orbital Hilbert space.

## II. SPIN-ORBIT-INTEGRATED ELECTRONIC STATES

### A. LDA+SO+ $U$ Band Structure

Since both on-site Coulomb interactions ( $U$ ) and SO couplings are expected to be important in the description of Ir 5d states, we examined the effect of on-site  $U$  and SO couplings separately and simultaneously on the electronic structure of  $\text{Sr}_2\text{IrO}_4$ . To identify the role of each term and the interplay between them, we carried out density-functional-theory (DFT) calculations within the local-density approximation (LDA), LDA including the SO coupling (LDA+SO), and LDA+ $U$  including the SO coupling (LDA+SO+ $U$ ), respectively. We calculated total energies and electronic band structures of  $\text{Sr}_2\text{IrO}_4$  for the structural parameters as obtained

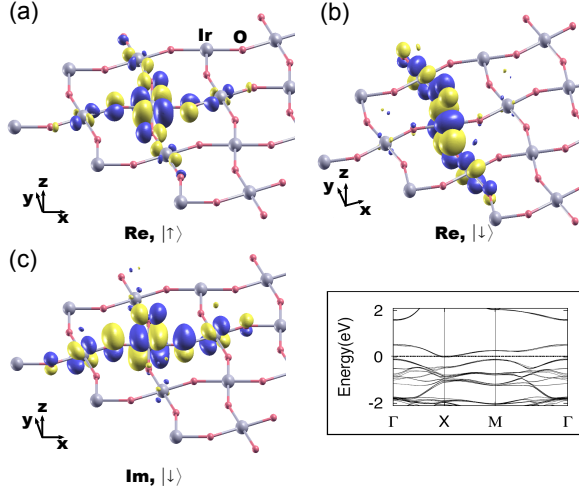


FIG. 1: (Color online) Calculated Wannier functions of the  $|j_{\text{eff}} = 1/2, +1/2\rangle$  state: (a) the real part of up-spin  $|\uparrow\rangle$  component, (b) the real part of the down-spin  $|\downarrow\rangle$  component, and (c) the imaginary part of the down-spin  $|\downarrow\rangle$  component. Blue (dark gray) and yellow (light gray) colors in the Wannier function represent negative and positive values respectively. The inset shows the LDA+SO+ $U$  band structure near  $E_F=0$  eV, emphasizing the “upper” and “lower” Hubbard band of the  $|j_{\text{eff}} = 1/2, m\rangle$  band above and below  $E_F$  respectively.

from the neutron powder diffraction data at 10 K<sup>15</sup>, which has a  $\text{K}_2\text{NiF}_4$ -type layered perovskite structure with the symmetry of the space group  $I4_1/acd$  reduced from  $I4/mmm$ , where  $\text{IrO}_6$  octahedra are rotated by about  $11^\circ$  around the  $c$ -axis of the unit cell. For the calculations, we used the DFT code, OpenMX<sup>16</sup>, based on the linear-combination-of-pseudo-atomic-orbitals method<sup>17</sup>, where both the LDA+ $U$  method<sup>18</sup> and the SO couplings were included via a relativistic  $j$ -dependent pseudo-potential scheme in the non-collinear DFT formalism<sup>19,20,21</sup>. Double valence and single polarization orbitals were used as a basis set, which were generated by a confinement potential scheme with cutoff radii of 8.0, 7.0 and 5.0 a.u. for Sr, Ir, and O atoms respectively. We used a  $(6 \times 6 \times 4)$   $\mathbf{k}$ -point grid for the  $\mathbf{k}$ -space integration.

Calculated LDA, LDA+SO, and LDA+SO+ $U$  band structures were presented in the previous work<sup>8</sup> where the results of the LDA+SO+ $U$  band structures of  $\text{Sr}_2\text{IrO}_4$  are well compared with those of angle resolved photoemission spectroscopy experiments. The LDA bands near the Fermi level ( $E_F$ ), as shown in Fig. 2(a) of Ref. [8], are almost identical to those of  $\text{Sr}_2\text{RhO}_4$ <sup>22</sup> which can be expected from the same  $d^5$  configuration of  $\text{Rh}^{4+}$  and  $\text{Ir}^{4+}$  and the same structural distortions, i.e., the rotations of  $\text{RhO}_6$  and  $\text{IrO}_6$  octahedra. The hybridization of  $d_{xy}$  and  $d_{x^2-y^2}$  due to the rotation of  $\text{IrO}_6$  octahedra pushes the  $d_{xy}$  band below  $E_F$ , similarly to the case of  $\text{Sr}_2\text{RhO}_4$ . Indeed the LDA Fermi surface of  $\text{Sr}_2\text{IrO}_4$  was found to be basically the same as that of  $\text{Sr}_2\text{RhO}_4$ <sup>22</sup>.

In the LDA band structure, the contribution of  $d_{xy}$  components above  $E_F$  are strongly suppressed relative to those of  $d_{yz}$  and  $d_{zx}$  states, whereas the Ir 5d bands ranging from  $-2.5$  eV to  $0.5$  eV are still dominated by the  $t_{2g}$  orbitals with a

TABLE I: Coefficients of the Wannier functions illustrated in Fig. 1: Only the coefficients from the center Ir are listed.

		up-spin		down-spin	
		Re	Im	Re	Im
Ir	$d_{z^2}$	0.00009	0.00009	0.00002	0.00001
	$d_{x^2-y^2}$	-0.09044	-0.01212	-0.00024	0.00016
	$d_{xy}$	0.32738	0.00000	0.00115	-0.00009
	$d_{yz}$	-0.00203	-0.00001	0.44105	0.05527
	$d_{zx}$	-0.00018	0.00183	-0.05450	0.44212

small admixture of  $d_{x^2-y^2}$ . On the other hand, however, when the SO coupling is included, a significant change of the wave function character occurs so that all three  $t_{2g}$  orbital components are almost equally distributed in the LDA+SO band structure. This change arises from the SO interactions acting on the  $t_{2g}$  manifold, which mixes up the  $d_{xy}$ ,  $d_{yz}$ , and  $d_{zx}$  orbitals. This qualitative change of the wave function character is an essence of the SO coupling action, which is related to the novel nature of the SO-integrated insulating ground state.

As shown in the inset of Fig. 1, an effective  $U = 2$  eV opens up a gap in the LDA+SO+ $U$  band structure and gives rise to the non-dispersive and parallel features of “upper” and “lower” Hubbard bands of the SO-integrated states, which are in excellent agreement with experimental observations<sup>8</sup>. It is remarkable to obtain an insulating ground state for the intermediate value of  $U$ , which is smaller than the band width of the  $t_{2g}$  manifold and the conventional  $U$  values of 3d TMOs. On the other hand, however, when we performed LDA+ $U$  calculations without the SO coupling, the on-site Coulomb interaction became *ineffective* due to the three-fold degeneracy of the Ir  $t_{2g}$  manifold crossing  $E_F$ <sup>23</sup>. Unless the degeneracy is broken, each band remains partially filled being far from the Mott instability. In our non-collinear DFT calculations, the SO coupling terms were solved in a completely non-perturbative way, whereas the Coulomb correlation effect were treated via the LDA+ $U$  method.

In order to examine the nature of the SO-integrated state, we constructed Wannier functions which can identify the orbital shape and bonding character of the “upper” and “lower” Hubbard bands of the SO-integrated states, as shown in the inset of Fig. 1. The Wannier functions were calculated for the  $t_{2g}$  manifold by employing the projection scheme<sup>24</sup>. The Wannier function illustrated in Fig. 1 corresponds to the single band above  $E_F$  of LDA+SO+ $U$  bands. As listed in Table I, the overall shape of the calculated Wannier function of Fig. 1 matches closely to the ideal  $j_{\text{eff}}=1/2$  state:

$$|j_{\text{eff}} = \frac{1}{2}, \pm \frac{1}{2}\rangle = \mp \frac{1}{\sqrt{3}} [(d_{xy})|\pm\rangle \pm (|d_{yz}\rangle \pm i|d_{zx}\rangle)|\mp\rangle], \quad (1)$$

where  $|\pm\rangle$  represent for the up-spin  $|\uparrow\rangle$  and down-spin  $|\downarrow\rangle$  states respectively. The agreement of its orbital components and their relative phases between the ideal state and the calculated Wannier function is another proof of the SO-integrated  $j_{\text{eff}}=1/2$  state. Here, for the sake of simplicity in the presenta-

tion, we chose a self-consistent solution with the spin quantization axis parallel to the  $z$ -axis.

### B. Tight-binding model

The physics of the LDA+SO+ $U$  results can be captured by a multi-band Hubbard model for the  $t_{2g}$  bands including the SO coupling term. The tight-binding (TB) bands for the  $t_{2g}$  manifold can be described by

$$\mathcal{H}_0 = \sum_{\langle ij \rangle \alpha \beta \sigma} t_{ij}^{\alpha \beta} c_{i\alpha\sigma}^\dagger c_{j\beta\sigma} + \sum_{i, a=d_{xy}} \Delta_t c_{ia\sigma}^\dagger c_{ja\sigma} + \lambda_{\text{SO}} \sum_i \mathbf{L}_i \cdot \mathbf{S}_i, \quad (2)$$

where  $\langle ij \rangle$  runs over the nearest neighbor pairs of sites  $i$  and  $j$  in the two-dimensional square lattice consisting of Ir ions,  $\alpha$  and  $\beta$  are indices for  $t_{2g}$  orbitals, i.e.,  $\{d_{xy}, d_{yz}, d_{zx}\}$ ,  $t_{ij}^{\alpha \beta}$  a hopping integral between  $|i\alpha\rangle$  and  $|j\beta\rangle$ ,  $\Delta_t$  a tetragonal crystal field splitting, i.e., an on-site energy difference of the  $d_{xy}$  orbital relative to  $d_{yz}$  and  $d_{zx}$ , and  $\lambda_{\text{SO}}$  the SO coupling parameter. In a simple square lattice of Ir ions,  $t_{ij}^{\alpha \beta}$  becomes a non-zero constant  $t_0$  only for  $(\alpha, \beta) = (d_{xy}, d_{xy}) = (d_{zx}, d_{zx})$  with  $j = i + \hat{x}$  and so on.

Starting from a set of  $\{\langle n_{i\tau\alpha\sigma} \rangle\}$  as mean-field parameters, we could obtain a self-consistent mean-field Hamiltonian within the  $t_{2g}$  subspace by  $\mathcal{H}_{t_{2g}} = \sum_{\mathbf{k}} C_{\mathbf{k}}^\dagger \hat{T}(\mathbf{k}) C_{\mathbf{k}}$  where  $C_{\mathbf{k}}$  has 12 components of  $\{c_{\mathbf{k}\tau\alpha\sigma} | \tau = A, B; \alpha = d_{xy}, d_{yz}, d_{zx}; \sigma = \uparrow, \downarrow\}$ . Here the site indices  $\tau = A, B$  are for the two inequivalent Ir sites. By choosing the basis in order of  $(c_{A d_{xy} \uparrow}, c_{A d_{yz} \downarrow}, c_{A d_{zx} \uparrow}, [A \rightarrow B], [\uparrow \leftrightarrow \downarrow])$ , we can find a block-diagonal  $12 \times 12$   $\hat{T}(\mathbf{k})$  matrix:

$$\hat{T}(\mathbf{k}) = \begin{pmatrix} \mathbf{D}_I^A & \mathbf{O}(\mathbf{k}) & 0 & 0 \\ \mathbf{O}^\dagger(\mathbf{k}) & \mathbf{D}_I^B & 0 & 0 \\ 0 & 0 & \mathbf{D}_{II}^A & \mathbf{O}(\mathbf{k}) \\ 0 & 0 & \mathbf{O}^\dagger(\mathbf{k}) & \mathbf{D}_{II}^B \end{pmatrix}. \quad (3)$$

Here the hopping integrals contribute to  $\mathbf{O}(\mathbf{k})$ :

$$\mathbf{O}(\mathbf{k}) = e^{-i \frac{k_x + k_y}{2}} \begin{pmatrix} -4t_0\gamma_{1\mathbf{k}} & 0 & 0 \\ 0 & -2t_0\gamma_{2\mathbf{k}} & 0 \\ 0 & 0 & -2t_0\gamma_{3\mathbf{k}} \end{pmatrix}, \quad (4)$$

where the non-zero hopping terms of  $t_0 = t_{d_{xy}} = t_{d_{yz}} = t_{d_{zx}}$  lead to the dispersions  $\gamma_{1\mathbf{k}} = \cos \frac{k_x}{2} \cos \frac{k_y}{2}$ ,  $\gamma_{2\mathbf{k}} = \cos \frac{k_x + k_y}{2}$ , and  $\gamma_{3\mathbf{k}} = \cos \frac{k_x - k_y}{2}$  for  $d_{xy}$ ,  $d_{yz}$ , and  $d_{zx}$  bands, respectively. The on-site Coulomb interaction  $U$  and the SO coupling  $\lambda_{\text{SO}}$  contribute to the diagonal term:

$$\mathbf{D}_I^\tau = \begin{pmatrix} \Delta_t + e_1 \gamma_{1\mathbf{k}}^2 - U \bar{n}_{\tau d_{xy} \uparrow} & \lambda_{\text{SO}}/2 & -i\lambda_{\text{SO}}/2 \\ \lambda_{\text{SO}}/2 & -U \bar{n}_{\tau d_{yz} \downarrow} & -i\lambda_{\text{SO}}/2 \\ i\lambda_{\text{SO}}/2 & i\lambda_{\text{SO}}/2 & -U \bar{n}_{\tau d_{zx} \downarrow} \end{pmatrix}, \quad (5)$$

and  $\mathbf{D}_{II}^\tau$  is a time-reversal partner of  $\mathbf{D}_I^\tau$ .

Despite of a large cubic crystal field splitting due to  $\Delta_c \approx 5$  eV between  $t_{2g}$  and  $e_g$ , there is a significant hybridization of  $d_{xy}$  and  $d_{x^2-y^2}$  due to the rotation of  $\text{IrO}_6$  octahedra. In order to describe both LDA and LDA+SO band structures properly,

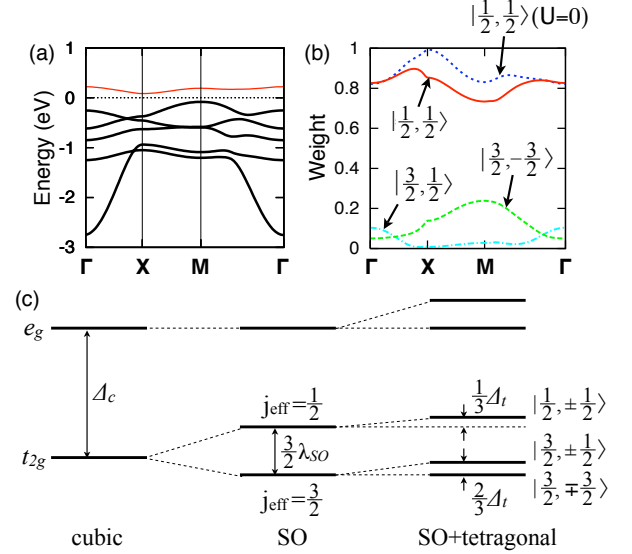


FIG. 2: (Color online) (a) Tight-binding band structure with  $(\lambda_{\text{SO}}, U) = (0.4 \text{ eV}, 2.0 \text{ eV})$ , which is well compared with the LDA+SO+ $U$  band structure of Fig. 1(c), (b) the decomposition of the “upper” Hubbard band wavefunction (marked by a thin (red) solid line in (a)) into the  $\{|j_{\text{eff}}, m_j\rangle\}$  basis, where the dotted line represents a  $|\frac{1}{2}, \frac{1}{2}\rangle$  component with  $U=0$ , and (c) a schematic energy diagram of the  $t_{2g}$  manifold in the atomic limit. Due to the large crystal field splitting by  $\Delta_c$ , the  $t_{2g}$  levels can be mapped into the effective  $l_{\text{eff}} = 1$  states where the tetragonal field splitting by  $\Delta_t$  is relatively insignificant.

the contribution of the  $d_{x^2-y^2}$  admixture is necessary to be included as a  $\mathbf{k}$ -dependent energy  $\Delta \varepsilon_{\mathbf{k} d_{xy}}$  for the  $d_{xy}$  band:  $\Delta \varepsilon_{\mathbf{k} d_{xy}} = e_1 \gamma_{1\mathbf{k}}^2$ . The best fit to the LDA bands was obtained by a set of parameters:  $\Delta_t = 0.15 \text{ eV}$ ,  $t_0 = 0.35 \text{ eV}$ , and  $e_1 = -1.5 \text{ eV}$ .

The solutions of our TB model including both SO coupling  $\lambda_{\text{SO}}$  and on-site Coulomb interaction  $U$  with different sets of parameters  $(\lambda_{\text{SO}}, U) = (0, 0)$ ,  $(0.4 \text{ eV}, 0)$  and  $(0.4 \text{ eV}, 2.0 \text{ eV})$  reproduce well the  $t_{2g}$  manifold of the LDA, LDA+SO, and LDA+SO+ $U$  bands, respectively. The self-consistent solution for  $(\lambda_{\text{SO}}, U) = (0.4 \text{ eV}, 2.0 \text{ eV})$  is shown in Fig. 2(a), which corresponds to the LDA+SO+ $U$  bands of the inset of Fig. 1.

In addition to the large crystal field splitting between  $e_g$  and  $t_{2g}$ , the  $t_{2g}$  manifold splits further into doubly degenerate  $j_{\text{eff}} = 1/2$  and quadruply degenerate  $j_{\text{eff}} = 3/2$  states due to SO coupling. The small tetragonal crystal field does not affect this configuration. A schematic energy level diagram shown in Fig. 2(c) was confirmed by the LDA and LDA+SO energy levels at the X point,<sup>8</sup> where the off-diagonal hopping matrix  $\mathbf{O}(\mathbf{k})$  in the TB model becomes zero. Even though the non-zero hopping terms away from X point may disturb the atomic picture, the SO coupling retains the anti-crossing between those levels which transform according to the same irreducible representation<sup>25</sup>. Consequently, the effective bandwidth of the half-filled  $j_{\text{eff}} = 1/2$  band becomes smaller than the modest value of on-site  $U$ . The decomposition of the “upper” Hubbard band wavefunction into the  $\{|j_{\text{eff}}, m_j\rangle\}$  basis clearly demonstrates the robustness of its  $j_{\text{eff}} = 1/2$  character

as shown in Fig. 2(b), whereas the  $j_{\text{eff}}=1/2$  weight for  $U = 2$  eV is slightly reduced from that of  $U = 0$ . Therefore it is reasonable to consider an effective Hamiltonian based on the  $j_{\text{eff}}=1/2$  single-band Hubbard model instead of the conventional  $S=1/2$  model:

$$\mathcal{H} = \sum_{\langle ij \rangle mm'} \bar{t}_{mm'}^{ij} d_{im}^\dagger d_{jm'} + \bar{U} \sum_i n_{di+1/2} n_{di-1/2}, \quad (6)$$

where  $d_{im}$  represents for the  $|j_{\text{eff}} = 1/2, m\rangle$  state at the site  $i$  with  $m, m' = \pm 1/2$  and  $n_{dim} = d_{im}^\dagger d_{im}$ .  $\bar{t}_{mm'}^{ij}$  and  $\bar{U}$  are effective hopping and on-site interaction parameters respectively.

### III. ANISOTROPIC EXCHANGE INTERACTIONS

#### A. Effective Exchange Hamiltonian

The  $j_{\text{eff}}=1/2$  single-band Hubbard model has an interesting feature in  $\bar{t}_{mm'}^{ij}$ , which originates from a peculiar nature of the spin-orbit integrated state in  $\text{Sr}_2\text{IrO}_4$ . In the strong SO coupling limit, the orbital wavefunctions of the  $|j_{\text{eff}} = 1/2, m\rangle$  state of Eq. (1) consists of the cubic harmonics with respect to the local coordinate axes. The rotation of the  $\text{IrO}_6$  octahedron results in a rotation of the  $|j_{\text{eff}} = 1/2, m\rangle$  state at each site  $i$ , thereby generating a spin-dependent hopping term. In  $\text{Sr}_2\text{IrO}_4$ , where the  $\text{IrO}_6$  octahedron is rotated by a angle  $\theta \approx 11^\circ$  about the  $c$ -axis, the effective hopping matrix  $\bar{t}_{mm'}^{ij}$  can be represented in terms of Pauli matrices by  $\bar{t}^{ij} = t_0 \mathbf{1} + i \bar{t}_1 \sigma_z$  where  $t_0$  and  $\bar{t}_1$  for  $(ij) = \hat{x}$  or  $\hat{y}$  become

$$\bar{t}_0^{\hat{x}/\hat{y}} = \frac{2t_0}{3} \cos \theta (2 \cos^4 \theta - 1) \quad (7)$$

$$\bar{t}_1^{\hat{x}/\hat{y}} = \frac{2t_0}{3} \sin \theta (2 \sin^4 \theta - 1). \quad (8)$$

At half-filling, an effective  $j_{\text{eff}}$ -spin Hamiltonian can be derived from the  $j_{\text{eff}}=1/2$  single-band Hubbard model of Eq. (6):

$$\mathcal{H}_{\text{spin}} = \sum_{\langle ij \rangle} [I_0 \mathbf{J}_i \cdot \mathbf{J}_j + I_1 J_{zi} J_{zj} + \mathbf{D}_{ij} \cdot \mathbf{J}_i \times \mathbf{J}_j] \quad (9)$$

where  $I_0 = 4(\bar{t}_0^2 - \bar{t}_1^2)/\bar{U}$ ,  $I_1 = 8\bar{t}_1^2/\bar{U}$ , and  $\mathbf{D}_{ij} = D_z \hat{\mathbf{z}}$  with  $D_z = 8\bar{t}_0 \bar{t}_1/\bar{U}$ . The first term is a conventional Heisenberg form of superexchange with the coupling constant  $I_0$ . The second and third terms are pseudo-dipolar and Dzyaloshinskii-Moriya (DM) antisymmetric exchange interactions, which originate from the pure imaginary hopping matrix element  $i\bar{t}_1$  between the neighboring  $|j_{\text{eff}} = 1/2, m\rangle$  states of rotated  $\text{IrO}_6$  octahedra.

#### B. Comparison with LDA+SO+U Results

From our LDA+SO+U calculations, the magnetic configuration of the insulating ground state was determined to be a

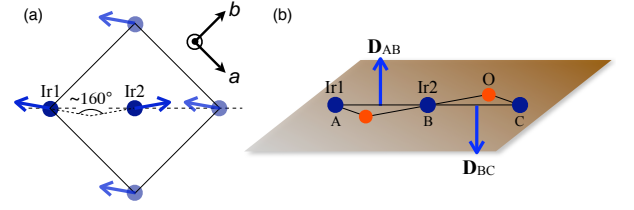


FIG. 3: (Color online) (a) Magnetic configuration and (b) DM vectors of the calculated LDA+SO+U ground state of  $\text{Sr}_2\text{IrO}_4$ . Blue arrows in (a) represent a non-collinear ordering of the local Ir moments, consisting of both spin and orbital components, in a canted AFM configuration. The DM vectors,  $\mathbf{D}_{AB}$  and  $\mathbf{D}_{BC}$ , in (b) are aligned along the  $c$ -axis with alternating signs and consistent with the Dzyaloshinskii-Moriya (DM) rule.

canted antiferromagnetic (AFM) state with the  $ab$ -plane as an easy plane. We found no preferred direction within the  $ab$ -plane. As illustrated in Fig. 3(a), there are two inequivalent Ir sites, i.e., Ir1 and Ir2 within the  $\sqrt{2} \times \sqrt{2}$  unit cell. It is found that the magnetic moment at each Ir site is  $0.36 \mu_B$  and both spin ( $0.10 \mu_B$ ) and orbital ( $0.26 \mu_B$ ) moments are parallel to each other. In addition, AFM moments are canted with the canting moment  $0.063 \mu_B$ , which is comparable to the single crystal measurement<sup>12</sup>.

According to the rule by Dzyaloshinskii and Moriya<sup>6</sup>, the direction of the vector  $\mathbf{D}_{ij}$  in  $\text{Sr}_2\text{IrO}_4$  should point to the  $c$ -axis due to a mirror plane containing Ir1-O-Ir2, as illustrated in Fig. 3(b). The directions of  $\mathbf{D}_{ij}$  can be represented by  $\mathbf{D}_{AB} = -\mathbf{D}_{BC} = (0, 0, d_c)$ , when considering the inversion symmetry at the site B, which gives the consistent results as the  $j_{\text{eff}}=1/2$  Hamiltonian of Eq. (9). From the LDA+SO+U calculations, it is concluded that the DM interaction is responsible for the magnetic anisotropy of  $\text{Sr}_2\text{IrO}_4$  with the  $ab$ -plane as an easy plane but isotropic within the  $ab$ -plane, whereas the single-ion anisotropy term has a negligible contribution. Contrary to the  $\text{La}_2\text{CuO}_4$ ,<sup>26</sup> which has no single-ion anisotropy due to the  $S=1/2$  ground state, the absence of the  $ab$ -plane anisotropy in  $\text{Sr}_2\text{IrO}_4$  is attributed to the tetragonal symmetry.

From the effective exchange Hamiltonian of Eq. (9), the ratio of  $D_z/I_0$ , which determines the spin canting angle, becomes  $|D_z/I_0| \approx \tan 2\theta$  for small  $\theta$ . In the strong SO coupling limit, the canting angle increases close to the rotation angle of  $\text{IrO}_6$  octahedra. We can estimate the magnitude of  $\mathbf{D}_{ij}$  to be  $|\mathbf{D}| \approx 3.8$  meV assuming the intersite superexchange interaction  $J \approx 10$  meV. This enormous DM interaction may well be related to the peculiar nature of the  $j_{\text{eff}}=1/2$  state. Contrary to the  $S=1/2$  counterpart of  $\text{La}_2\text{CuO}_4$ ,<sup>26</sup> the  $j_{\text{eff}}=1/2$  state has an open-shell of the  $l = 1$  orbital where the non-perturbative ground state of  $j_{\text{eff}}=1/2$  spin-orbit coupled state contribute to the DM term. Although the small magnetic moment of Ir observed in experiments was attributed to the effective moment the  $j_{\text{eff}}=1/2$  state, one can expect possible contributions from the  $j=1/2$  quantum-fluctuation. Nevertheless, since  $j_{\text{eff}}=1/2$  state is an eigenstate of the fictitious angular momentum  $\mathbf{J}_{\text{eff}} = \mathbf{L}_{\text{eff}} + \mathbf{S} = -\mathbf{L} + \mathbf{S}$ , the orbital contribution to the magnetic moment needs a careful interpretation<sup>8</sup>.

#### IV. CONCLUSIONS

In summary, we presented the effective  $j_{\text{eff}}$ -spin model Hamiltonian for  $\text{Sr}_2\text{IrO}_4$ . The strong SO interaction combined with the large crystal field splitting in  $5d$  TMOs introduces a unique form of the spin-orbit integrated band state at  $E_F$ , leading to an effective insulating ground state of  $j_{\text{eff}}=1/2$  quantum magnet. The observed weak ferromagnetism is understood by the DM anisotropic exchange interaction where the effective exchange interactions arise from the full spin-orbital Hilbert space. We hope that our prototype model of the spin-orbit integrated magnetism is useful for the study of various spin-orbit entangled physics. By taking an analogy of the high  $T_c$

superconductors as a doped  $S=1/2$  quantum magnet, it will be interesting to observe a doped  $j=1/2$  quantum magnet as a spin-orbit integrated correlated electron system.

#### Acknowledgments

We are grateful to Profs. T. W. Noh and J. H. Park for valuable comments and suggestions. This work was supported by the KOSEF through the ARP (R17-2008-033-01000-0). We also acknowledge the computing resources support by the KISTI Supercomputing Center.

---

\* Corresponding author. Electronic address: jyu@snu.ac.kr

<sup>1</sup> Hubbard, Proc. Roy. Soc. **A276**, 238 (1963).

<sup>2</sup> S. Maekawa, T. Tohyama, S. E. Barnes, S. Ishihara, W. Koshibae, and G. Khaliullin, *Physics of Transition Metal Oxides*, vol. 144 of *Springer Series in Solid State Sciences* (Springer-Verlag, Berlin, 2004).

<sup>3</sup> G. Jackeli and G. Khaliullin, arXiv.org:0809.4658 (2008).

<sup>4</sup> J.-S. Zhou, J. B. Goodenough, J.-Q. Yan, and Y. Ren, Phys. Rev. Lett. **99**, 156401 (2007).

<sup>5</sup> A. M. Oleś, P. Horsch, L. F. Feiner, and G. Khaliullin, Phys. Rev. Lett. **96**, 147205 (2006).

<sup>6</sup> K. Yosida, *Theory of Magnetism*, vol. 122 of *Springer Series in Solid State Sciences* (Springer-Verlag, Berlin, 1996).

<sup>7</sup> L. F. Mattheiss, Phys. Rev. B **13**, 2433 (1976).

<sup>8</sup> B. J. Kim, H. Jin, S. J. Moon, J.-Y. Kim, B.-G. Park, C. S. Leem, J. Yu, T. W. Noh, C. Kim, S.-J. Oh, et al., Phys. Rev. Lett. **101**, 076402 (2008).

<sup>9</sup> S. J. Moon, H. Jin, K. W. Kim, W. S. Choi, Y. S. Lee, J. Yu, G. Cao, A. Sumi, H. Funakubo, C. Bernhard, et al., Phys. Rev. Lett. **101**, 226402 (2008).

<sup>10</sup> M. K. Crawford, M. A. Subramanian, R. L. Harlow, J. A. Fernandez-Baca, Z. R. Wang, and D. C. Johnston, Phys. Rev. B **49**, 9198 (1994).

<sup>11</sup> T. Shimura, Y. Inaguma, T. Nakamura, M. Itoh, and Y. Morii, Phys. Rev. B **52**, 9143 (1995).

<sup>12</sup> G. Cao, J. Bolivar, S. McCall, J. E. Crow, and R. P. Guertin, Phys. Rev. B **57**, R11039 (1998).

<sup>13</sup> N. S. Kini, A. M. Strydom, H. S. Jeevan, C. Geibel, and S. Ramakrishnan, J. Phys.: Condens. Matter **18**, 8205 (2006).

<sup>14</sup> S. J. Moon, M. W. Kim, K. W. Kim, Y. S. Lee, J.-Y. Kim, J.-H.

Park, B. J. Kim, S.-J. Oh, S. Nakatsuji, Y. Maeno, et al., Phys. Rev. B **74**, 113104 (2006).

<sup>15</sup> Q. Huang, J. L. Soubeyroux, O. Chmaissem, I. N. Sora, A. Santoro, R. J. Cava, J. J. Krajewski, and W. F. P. Jr., J. of Solid State Chem. **112**, 355 (1994).

<sup>16</sup> The DFT code, OpenMX, is available at the web site (<http://www.openmx-square.org>) in the constitution of the GNU General Public License.

<sup>17</sup> T. Ozaki, Phys. Rev. B **67**, 155108 (2003).

<sup>18</sup> M. J. Han, T. Ozaki, and J. Yu, Phys. Rev. B **73**, 045110 (2006).

<sup>19</sup> A. H. MacDonald and S. H. Vosko, J. Phys. C: Solid State Phys. **12**, 2977 (1979).

<sup>20</sup> G. B. Bachelet, D. R. Hamann, and M. Schlüter, Phys. Rev. B **26**, 4199 (1982).

<sup>21</sup> G. Theurich and N. A. Hill, Phys. Rev. B **64**, 073106 (2001).

<sup>22</sup> B. J. Kim, J. Yu, H. Koh, I. Nagai, S. I. Ikeda, S.-J. Oh, and C. Kim, Phys. Rev. Lett. **97**, 106401 (2006).

<sup>23</sup> We have tried an unphysically large  $U=6\text{eV}$  in LDA+ $U$  without the SO coupling and then obtained an insulating ground state with a large spin and orbital polarization, which may lead to a lattice distortion.

<sup>24</sup> V. I. Anisimov, D. E. Kondakov, A. V. Kozhevnikov, I. A. Nekrasov, Z. V. Pchelkina, J. W. Allen, S.-K. Mo, H.-D. Kim, P. Metcalf, S. Suga, et al., Phys. Rev. B **71**, 125119 (2005).

<sup>25</sup> R. Winkler, *Spin-orbit coupling effects in two-dimensional electron and hole systems* (Springer-Verlag, Berlin, 2003).

<sup>26</sup> S.-W. Cheong, J. D. Thompson, and Z. Fisk, Phys. Rev. B **39**, 4395 (1989).